

Supporting Information

Revisiting the phosphonium salts chemistry for P-doped carbons synthesis: toward high phosphorus contents and beyond phosphate environment

Rémi F. André,^{1,*} Christel Gervais,² Hannes Zschiesche,¹ Teodor Jianu,¹ Nieves López-Salas,^{1,3}
Markus Antonietti,^{1,*} Mateusz Odziomek^{1,*}

¹ Colloid Chemistry Department, Max Planck Institute of Colloids and Interfaces (MPIKG), 14476 Potsdam, Germany

² Sorbonne Université, CNRS, Laboratoire de Chimie de la Matière Condensée de Paris (LCMCP), 4 place Jussieu, 75005 Paris, France

³ Chair of Sustainable Materials Chemistry, Paderborn University, Warburger Strasse 100, 33098, Paderborn, Germany

*Corresponding author. E-mail: remi.andre@mpikg.mpg.de

Table of contents

A.	Materials syntheses and characterization	2
A.1.	Condensation THPC-urea: neat vs. with salts	2
A.2.	X-ray diffraction experiments	6
A.3.	Infrared spectroscopy.....	9
A.4.	Solid-state NMR experiments	11
A.5.	XPS experiments.....	13
B.	Oxidative dehydrogenation.....	15
B.1.	Indoline aromatization	15
B.2.	Substrate screening.....	17
C.	Model materials.....	24

A. Materials syntheses and characterization

A.1. Condensation THPC-urea: neat vs. with salts

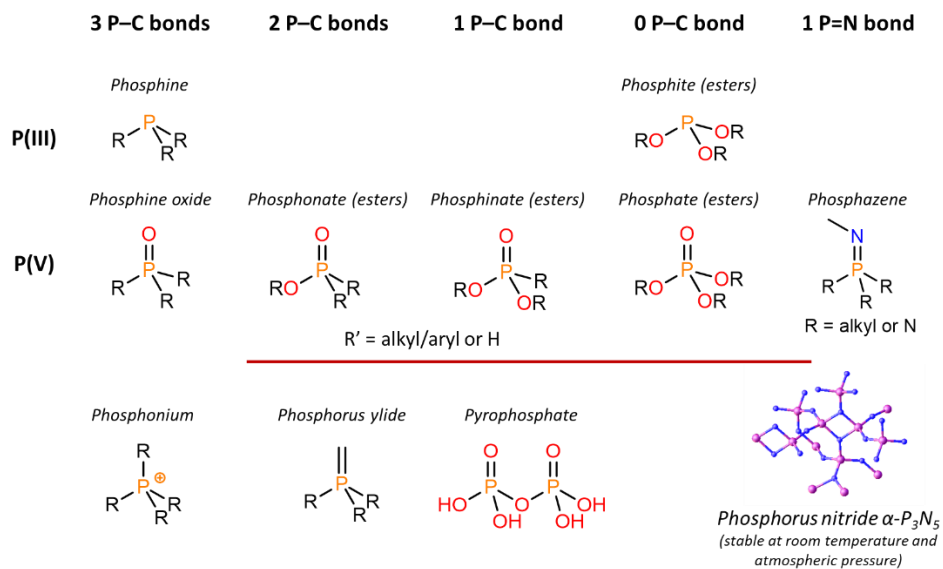


Figure S1. Nomenclature of P-containing groups encountered in P-doped carbonaceous materials and common precursors.

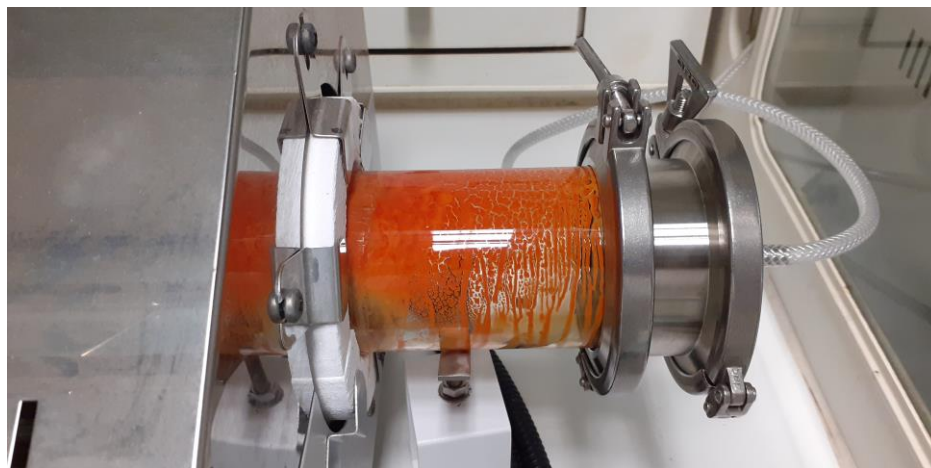


Figure S2. Digital photograph of the downstream of the synthesis of P/N co-doped carbon in a tubular oven (heating ramp of 2.5 °C/min).

Table S1. Yields of syntheses. The mass yield is given vs. the mass of [THPC 80 wt.% + 2 urea] (1191 mg and 600 mg respectively).

Sample	Mass mg	Yield %	C yield %	P yield %
TU- <i>no salt</i> -600	420	23	48	54
TU-Ca6-1	883	49	53	65
TU-Ca6-2	822	46	49	65
TU-Ca6-5	604	34	51	47
TU-Ca6-10	444	25	42	33
TU- <i>no salt</i> -800	369	21	60	45
TU-Ca8-1	515	29	59	61
TU-Ca8-2	459	26	67	48
TU-Ca8-3	444	25	70	50
TU-Ca8-5	360	20	59	42
TU-Ca8-10	290	16	50	28
TU-Ca8-20	240	13	41	20

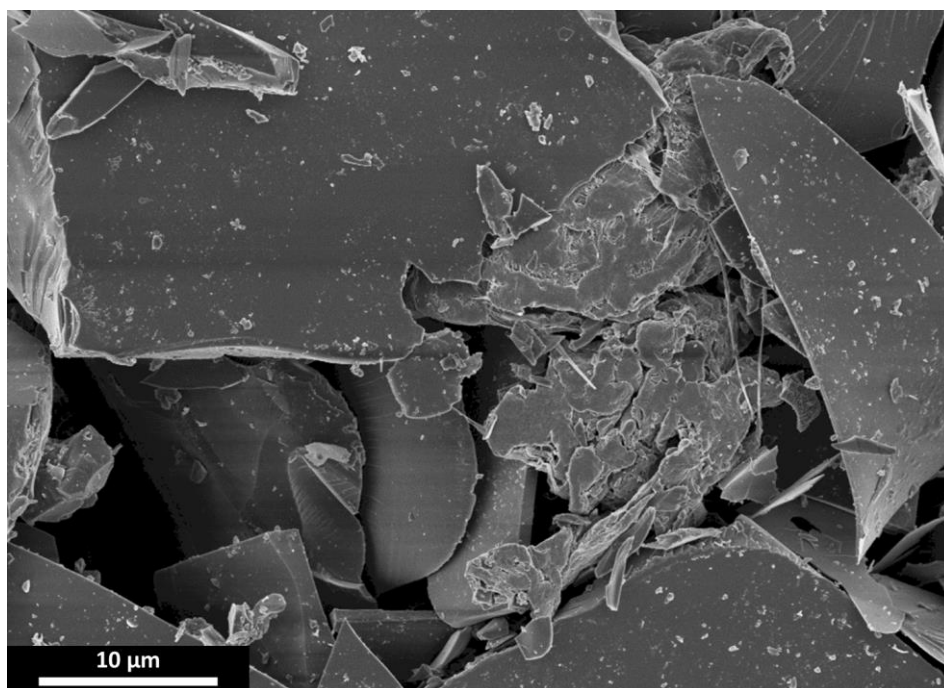


Figure S3. SEM picture of sample [THPC + 2 urea] carbonized in absence of salt at 600 °C.

On one hand, magnesium $\text{MgCl}_2 \cdot 6\text{H}_2\text{O}$ led to a material of low phosphorus content *ca.* 6 wt.% and with only traces of nitrogen. On the other hand, $\text{CaCl}_2 \cdot 4\text{H}_2\text{O}$ and $\text{ZnCl}_2 \cdot 4\text{H}_2\text{O}$ generated materials of similar porosity and P content *ca.* 18 wt.%, incidentally unveiling an unexpected difference between Mg^{2+} and Ca^{2+} salts. Calcium chloride was used in the following considering its lower corrosiveness, price and volatility than zinc chloride ($T_{\text{boiling}}(\text{ZnCl}_2) = 732 \text{ }^\circ\text{C}$ vs. $T_{\text{boiling}}(\text{CaCl}_2) = 1935 \text{ }^\circ\text{C}$).

Table S2. Composition and morphology characteristics of the samples synthesized in molten salt hydrates. Samples prepared at 600 °C with a metal chloride to THPC ratio of 10. [a] Determined by ICP-OES with a typical error bar of 0.5 wt.%. [b,c] Determined from N_2 adsorption isotherm at 77 K for $0.03 < P/P_0 < 0.15$ for S_{BET} , and at $P/P_0 = 0.95$ for total pore volume V_T (pores smaller than 40 nm in diameter). [d] Samples synthesized without salt could not be effectively digested for ICP analysis, the reported P contents correspond to the ones from EDX analysis. [e] Material produced in triplicate with identical results.

Sample	C yield %	P content ^[a] wt. %	P yield %	S_{BET} ^[b] $\text{m}^2 \cdot \text{g}^{-1}$	V_T ^[c] $\text{mL} \cdot \text{g}^{-1}$
TU- <i>no salt</i> -600	48	20 ^[d]	54	< 5	< 0.01
TU-Zn6-10	48	18.2	51	89	0.08
TU-Mg6-10 ^[e]	20	6.4	4	524	0.71
TU-Ca6-10	45	17.3	33	172	0.36

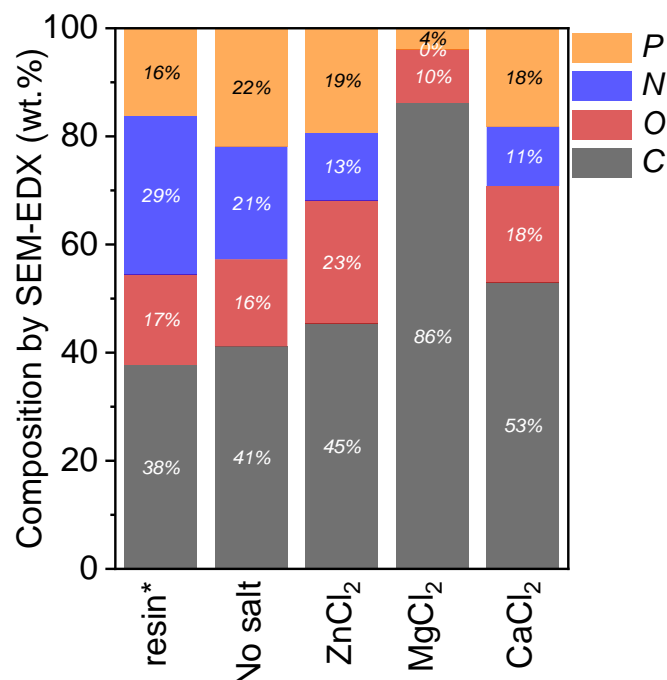


Figure S4. Elemental composition of samples synthesized at 600 °C according to SEM-EDX.

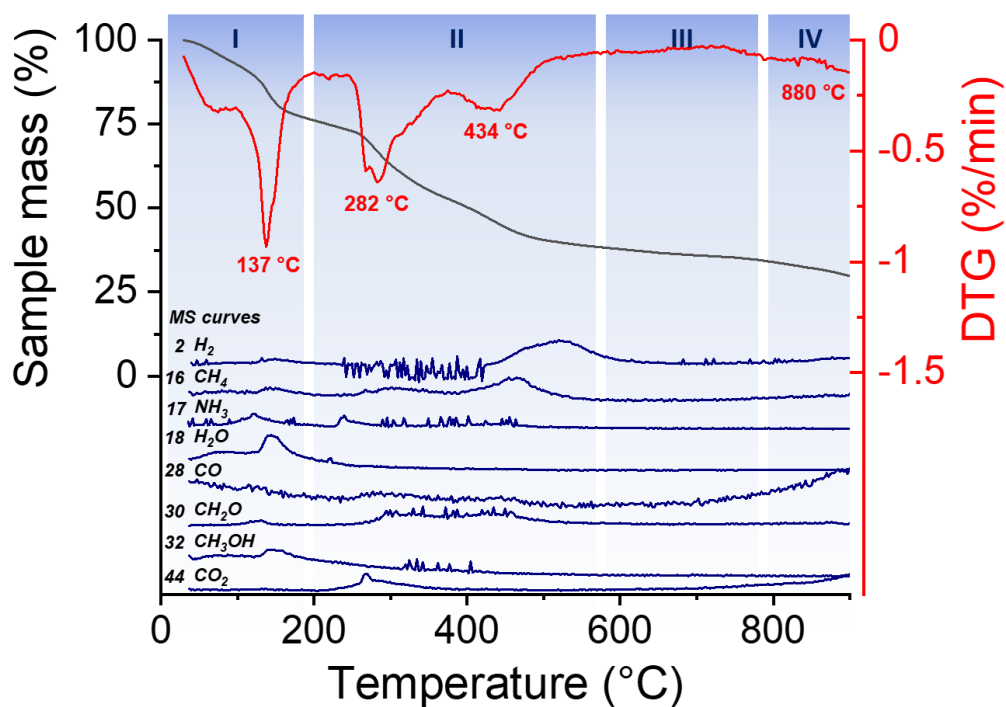


Figure S5. TGA-MS curves of carbonization of [THPC + 2 urea + 2CaCl₂·2H₂O] under Helium (heating ramp of 2.5 °C/min). Sample mass (black) and derivative (red), with corresponding MS curves (arbitrary units) at different m/z (blue), Suggestions of fragments are given for MS. The slight shift of the peak temperatures (137 °C, 282 °C and 434 °C) when compared with TGA-MS in absence of CaCl₂ is presumably due to a stabilizing effect from the CaCl₂ salt toward liquid water molecules and to the embedment of the carbon materials in CaCl₂, thus delaying its transformation.

A.2. X-ray diffraction experiments

The characteristic pattern of anhydrous CaCl_2 (Hydrophilite, ICDD N° 00-024-0223) rapidly evolved to $\text{CaCl}_2 \cdot 2\text{H}_2\text{O}$ under the X-ray beam (Sinjarite, ICDD N° 04-010-1481). The only crystalline phase detected in TU-Ca8-1 is a calcium chloro-phosphate $\text{Ca}_2(\text{PO}_4)\text{Cl}$ (Goryainovite, ICDD N° 04-009-8757), but an increase of the CaCl_2 content did not generate further this phase, and CaCl_2 was recovered instead, in addition of traces of $\text{Ca}_2(\text{PO}_4)\text{Cl}$. The chloro-phosphate presumably originates from phosphorus-containing groups exposed at the surface of the so-formed carbonaceous material or from an unpolymerized phosphorus side products. Although water washing was sufficient to remove CaCl_2 , washing away all $\text{Ca}_2(\text{PO}_4)\text{Cl}$ required 1 M HCl.

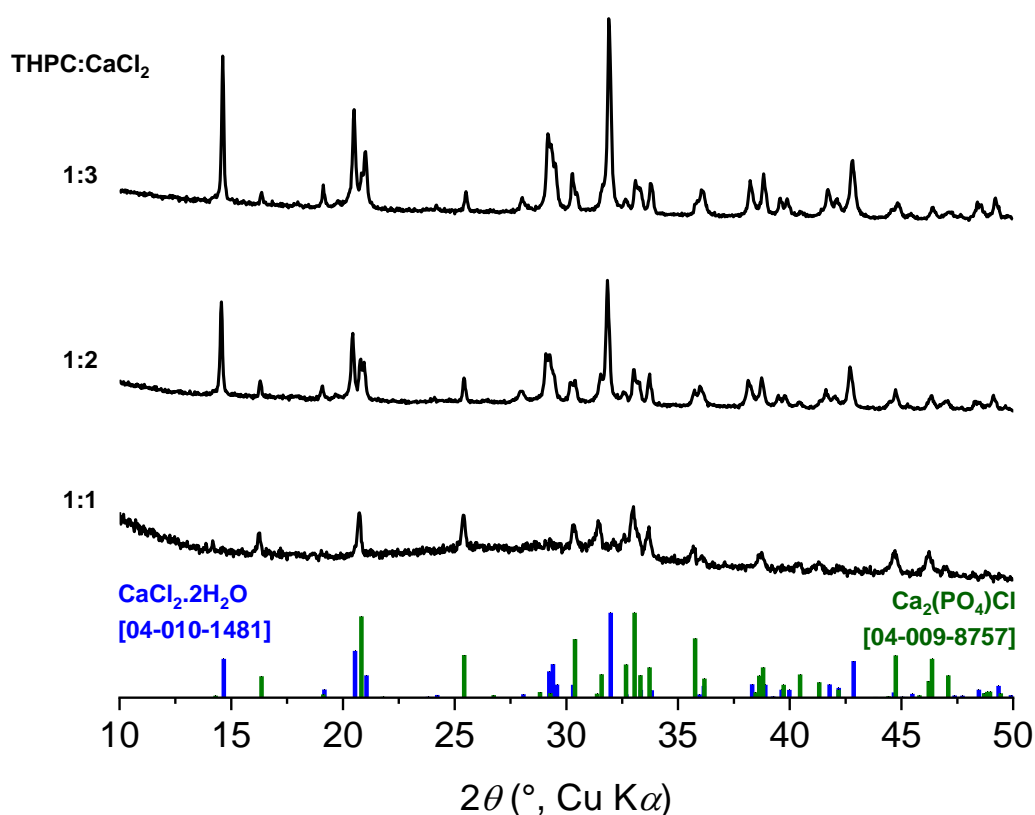


Figure S6. X-Ray Powder diffraction patterns of samples synthesized at 800 °C in $\text{CaCl}_2 \cdot 4\text{H}_2\text{O}$ with varying THPC: CaCl_2 molar ratios before washing.

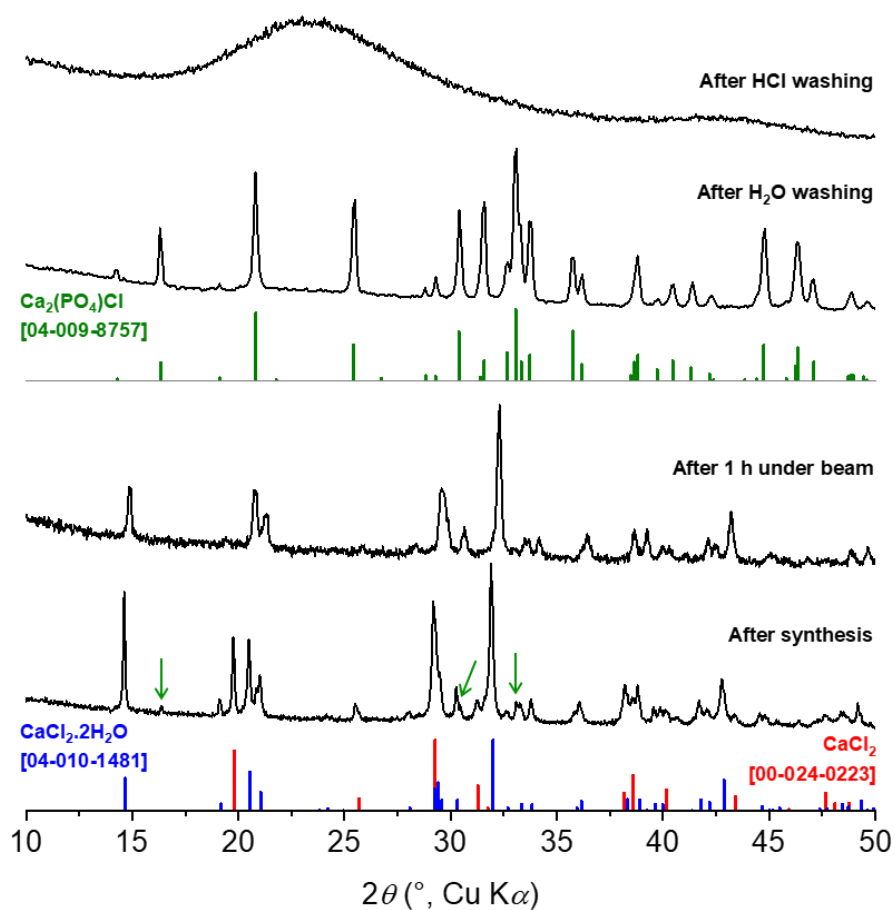


Figure S7. X-Ray Powder diffraction patterns of the sample synthesized at 800 °C in $\text{CaCl}_2 \cdot 4\text{H}_2\text{O}$ (TU-Ca8-5) at different stages. From bottom to top: immediately after removal from oven, after 1 h (the sample got soaked with water hence a not perfectly flat surface and broadening of the peaks), after water washing and after acidic washing (HCl 1 M). A quick scan was used as the sample soaks with water upon X-ray beam exposure. Green arrows indicate the traces of $\text{Ca}_2(\text{PO}_4)\text{Cl}$.

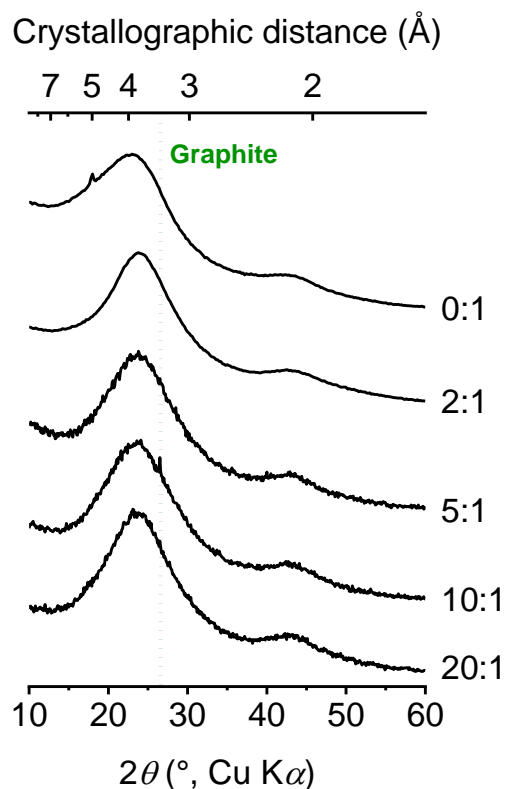


Figure S8. X-Ray Powder diffraction patterns of samples synthesized at 800 °C in $\text{CaCl}_2 \cdot 4\text{H}_2\text{O}$ with varying THPC: CaCl_2 molar ratios after washing. The phosphorus atomic size is significantly larger than that of carbon. Besides, the P–C bond length and C–P–C angle do not match with graphitic structures, we therefore assume that the P atoms are present as bulky edge terminations or ridges in the planes. Such groups cause a local geometric distortion of the interlayer packing, hence a larger interlayer distance.

A.3. Infrared spectroscopy

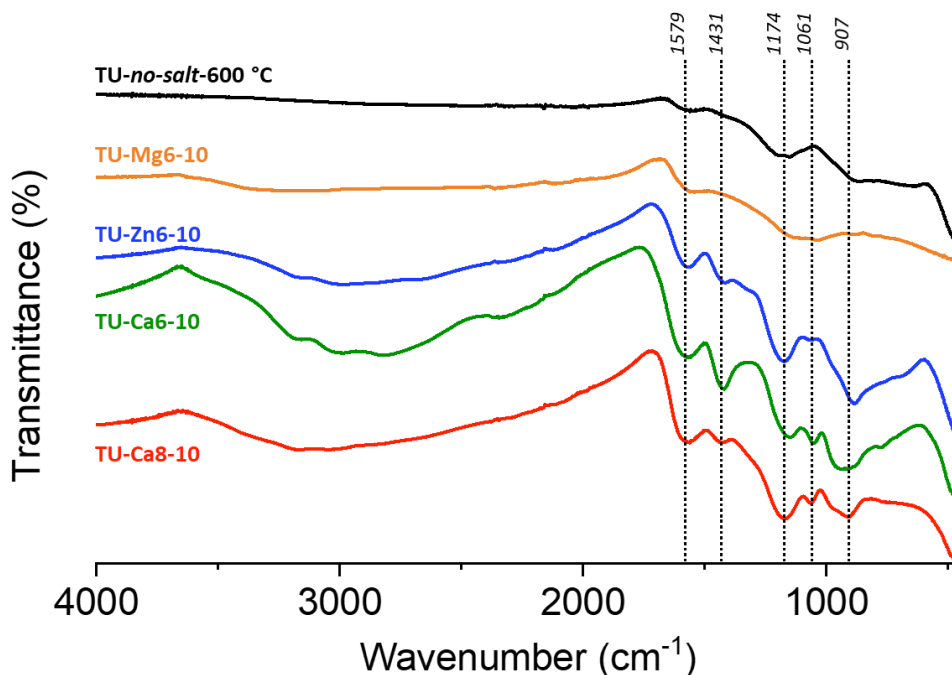


Figure S9. Attenuated Total Reflectance Fourier Transform Infrared (ATR-FTIR) spectra of samples synthesized at various temperatures and in presence of different metal salts. The band at 1431 cm^{-1} , absent in nitrogen-free TU-Mg6-10, likely sign the presence of C=N/C–N or P=N/P–N bonds. The prominent absorption band at 1174 cm^{-1} is attributed to the P=O stretching. Its position rather suggests a phosphinic acid $[(\text{HO})\text{R}_2\text{PO}]$ environment than a phosphate $[(\text{OR})_3\text{PO}]$ or phosphonate $[(\text{OR})_2\text{RPO}]$ one which would be more up-shifted ($> 1200\text{ cm}^{-1}$).¹ The bands at 907 cm^{-1} and 1061 cm^{-1} are usually attributed to P–O stretching vibrations.² The absence of band at $1650\text{--}1750\text{ cm}^{-1}$ reveals the absence of C=O groups. The strong band at 1579 cm^{-1} is due to aromatic ring stretching vibrations (C=C, C=N) absorption.

¹ Katzin, L.I., G.W. Mason, and D.F. Peppard, *Infrared spectral observation on the P=O group vibration of some homogeneous series of organic derivatives of P (V)*. *Spectrochimica Acta Part A: Molecular Spectroscopy*, 1978. **34**(1): p. 57-61.

² Puziy, A.M., et al., *Phosphorus-containing carbons: Preparation, properties and utilization*. *Carbon*, 2020. **157**: p. 796-846.

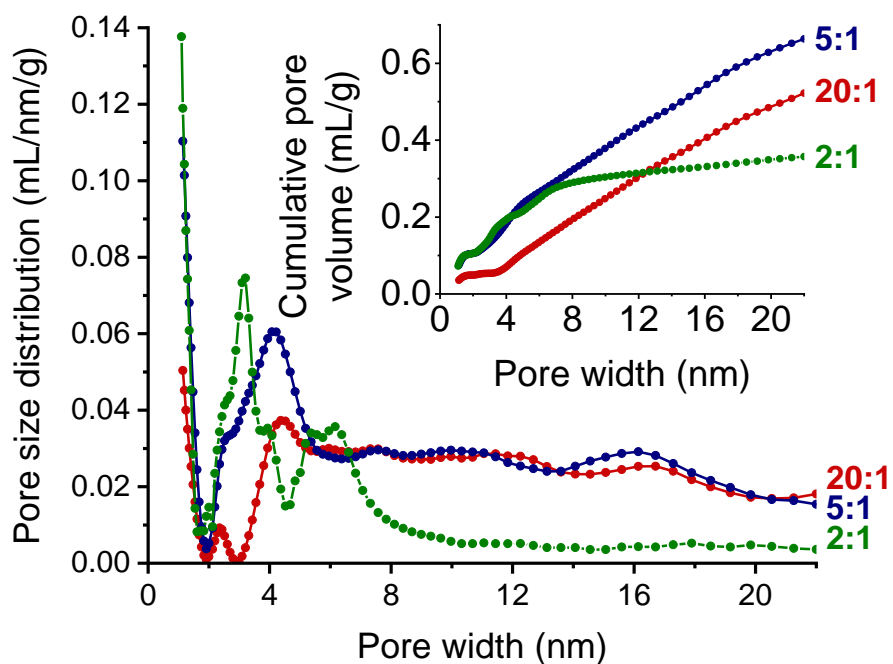


Figure S10. Pore size distributions. Note that the QSDFT model was initially developed for carbons with limited amounts of heteroatoms, and the quantitative values of these PSD should therefore be considered with caution as higher-than-carbon surface energies or heterogeneity of functionality are not considered in the model.

A.4. Solid-state NMR experiments

Table S3. Reported ^1H and ^{31}P chemical shifts of THPC, THP, THPO and THPOH in liquid state NMR.³

	^1H NMR	^{31}P NMR
$(\text{HO}-\text{CH}_2)_4\text{P}^+ \text{Cl}^-$	4.6 ppm	26 ppm
$(\text{HO}-\text{CH}_2)_3\text{P}$	4.0 ppm	-24 ppm
$(\text{HO}-\text{CH}_2)_3\text{P}=\text{O}$	4.1 ppm	49 ppm
$(\text{HO}-\text{CH}_2)_4\text{P}^+ \text{OH}^-$	3.6 ppm	36 ppm

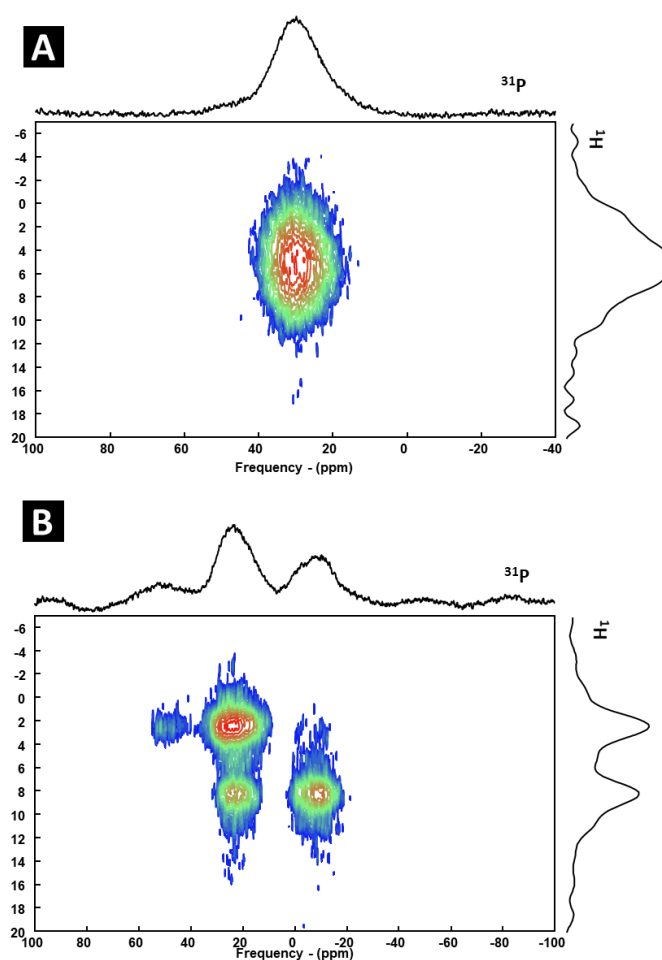


Figure S11. ^{31}P - ^1H CP MAS HETCOR NMR spectra of samples (A) TU-200 °C and (B) TU-350 °C, acquired at 16.4 T.

³ Mateo, J.M., et al., *Insights into the mechanism of the formation of noble metal nanoparticles by in situ NMR spectroscopy*. *Nanoscale Adv*, 2020. **2**(9): p. 3954-3962

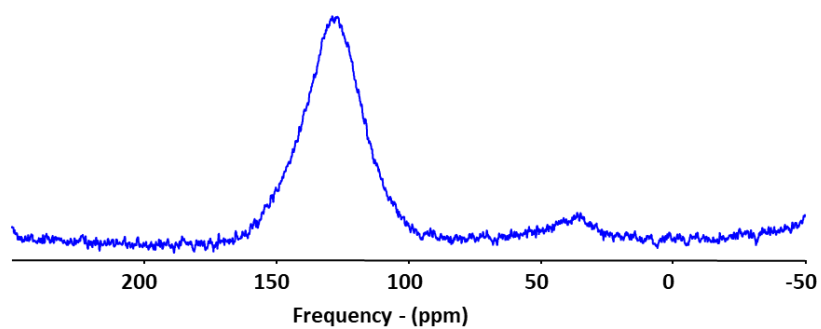


Figure S12. ^{13}C CP MAS NMR spectrum of sample TU-600 °C (no salt), acquired at 7 T.

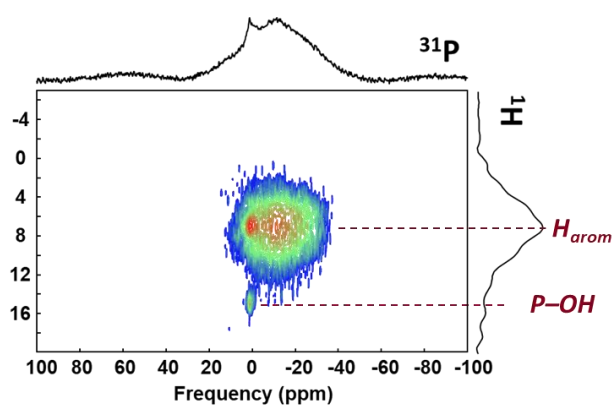


Figure S13. $^{31}\text{P}\{-^1\text{H}\}$ CP MAS HETCOR NMR spectrum of sample TU-600 °C (no CaCl_2), acquired at 16.4 T.

A.5. XPS experiments

The evolution of the C 1s spectra is typical of carbon materials formation with an important decrease of the C–X (286.2 eV) and X–C=X (289.1 eV) components (X = O, N or P here) upon thermal treatment and decomposition of surface alcohols and urea groups. The deconvolution of N 1s spectra in pyridinic-N (398.8 eV), amine-N (399.8 eV), pyrrolic-N (400.5 eV), graphitic-N (401.9 eV) and N-oxide (404.0 eV) confirms the main contribution in the resin state is the amine type (derived from urea condensation) while more diversity is present in the calcined materials with nitrogen in aromatic structures. Few reference data are available as to P–N and P=N bonds, except for pentavalent phosphazene structures –N–PR₂=N– exhibiting a signal *ca.* 399 eV,⁴ and P₃N₅ *ca.* 398 eV,⁵ which could both fit with the present spectra.

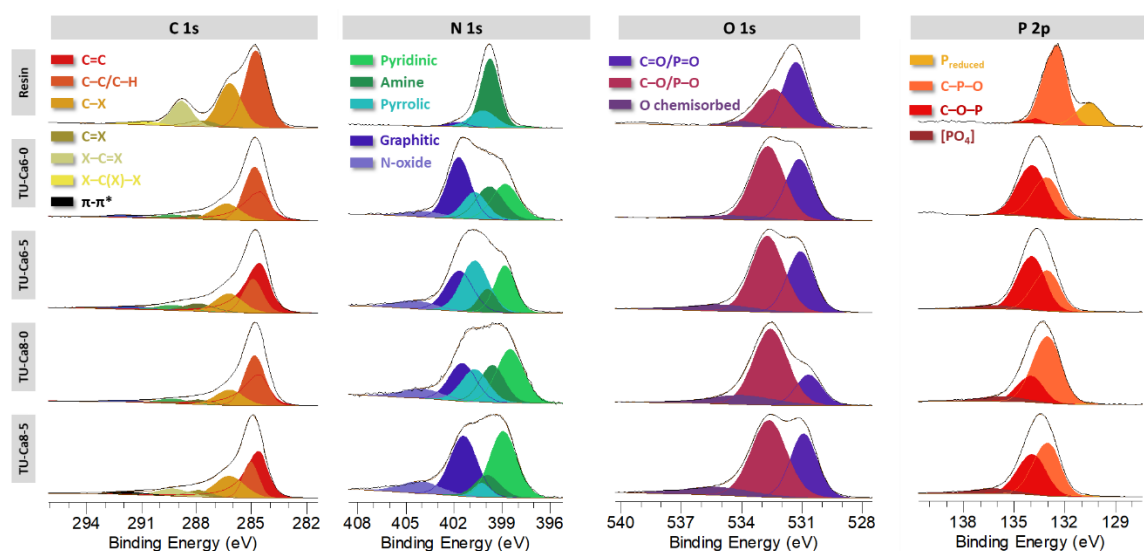


Figure S14. X-ray photoelectron spectra (C 1s, N 1s, O 1s and P 2p) with proposed deconvolution of the resin obtained at 200 °C in absence of CaCl₂, TU-Ca6-0, TU-Ca6-5, TU-Ca8-0 and TU-Ca8-5 (from top to bottom).

⁴ Vassileva, P., et al., *XPS determination of the binding energies of phosphorus and nitrogen in phosphazenes*. Journal of Materials Science, 2004. **39**(9): p. 3201-3202.

⁵ Vepřek, S., et al., *Preparation and properties of amorphous phosphorus nitride prepared in a low-pressure plasma*. Philosophical Magazine B, 2006. **43**(3): p. 527-547.

Table S4. XPS peak positions and widths for deconvolution of C 1s, N 1s, O 1s and P 2p regions. [a] Asymmetric peak fitted by a LA(1.53, 243) function. [b] Element X may be oxygen, nitrogen or phosphorus. [c] The X–C(X)–X component was considered only for the resin at 200 °C, the π – π^* one only for the samples calcined at 600 °C/800 °C. [d] P 2p signals are composed of doublets, 2p_{1/2} and 2p_{3/2}, in a 1:2 intensity ratio and with a spin-orbit coupling of 0.84 eV. Reported values in B.E. correspond to the P 2p_{3/2} contribution.

Component	B. E. (eV)	FWHM (eV)
C 1s		
C=C ^[a]	284.5 ± 0.2	0.5 – 2.0
C–C	284.8 ± 0.2	0.5 – 2.2
C–X ^[b]	286.2 ± 0.2	0.5 – 2.2
C=X ^[b]	287.8 ± 0.3	0.5 – 2.2
X–C=X ^[b]	289.1 ± 0.3	0.5 – 2.2
X–C(X)–X ^[b,c]	291.0	
π – π^* (shake up) ^[c]	291.7 ± 0.5	1.0 – 6.0
N 1s		
N _{pyridinic}	398.5 ± 0.5	1.1 – 2.0
N _{pyridonic/Namine}	399.8 ± 0.2	1.1 – 2.0
N _{pyrrolic}	400.3 ± 0.4	1.1 – 2.0
N _{graphitic}	401.7 ± 0.5	1.1 – 2.0
N _{oxide}	403.2 ± 0.8	1.1 – 3.0
O 1s		
C=O/P=O	531.0 ± 0.4	1.0 – 2.0
C–O/P–O	532.6 ± 0.3	1.0 – 2.0
chemisorbed [O]/H ₂ O	536 ± 1.2	1.0 – 6.0
P 2p ^[d]		
P _{reduced}	130.3	
C–P–O	132.8 ± 0.4	0.5 – 3.0
C–O–P	133.9 ± 0.4	0.5 – 3.0
[PO ₄]	135.0 ± 1.0	

B. Oxidative dehydrogenation

B.1. Indoline aromatization

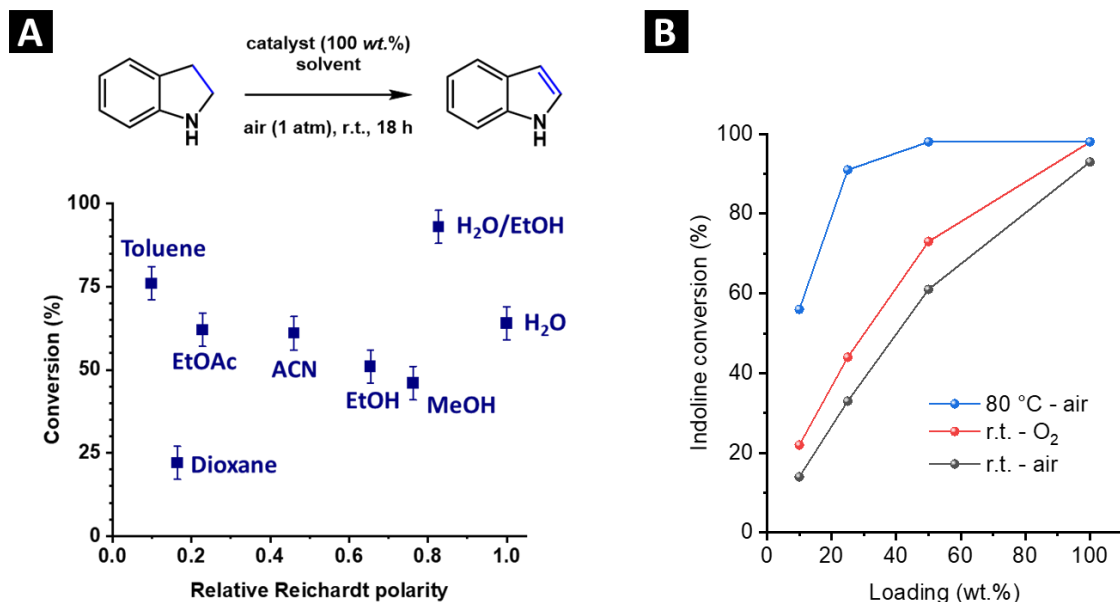


Figure S15. (A) Impact of relative polarity of the solvent on indoline conversion. No trend clearly emerged. Reaction conditions: indoline (28 μ L, 0.25 mmol), solvent (2.5 mL), catalyst (30 mg), air 1 bar, r.t., 18 h. Error bars denote the typical uncertainty due to quantification by ^1H NMR. (B) Impact of catalyst loading on conversion at r.t./80 °C and in air/O₂ atmosphere.

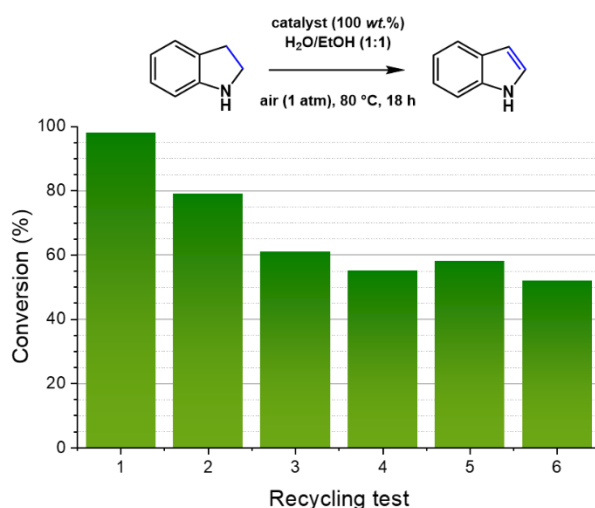


Figure S16. Indoline conversion over gram-scale recycling tests. The amount of indoline is kept constant (10 mmol) and the mass of catalyst slightly decreased due to losses upon recovery (1: 1200 mg, 2: 1180 mg, 3: 1120 mg, 4: 1090 mg, 5: 1050 mg, 6: 1020 mg).

- *No H₂O₂ generation upon catalysis*

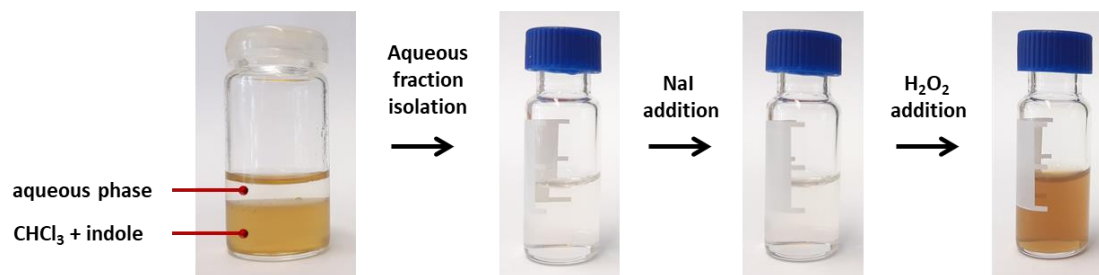


Figure S17. Hydrogen peroxide presence test. A fraction of the reaction [10 wt.% catalyst, 80 °C in air] was filtered and extracted with CHCl₃. The aqueous phase was further tested for the presence of H₂O₂ by addition of I⁻. The absence of deep brown coloration, characteristic of the triiodide ion I₃⁻ generated in presence of oxidants indicates a negative result.

B.2. Substrate screening

All ^1H NMR spectra displayed in the following correspond to the experiments of the screening experiments. They were acquired from an aliquot of the crude diluted in CDCl_3 (7.26 ppm).

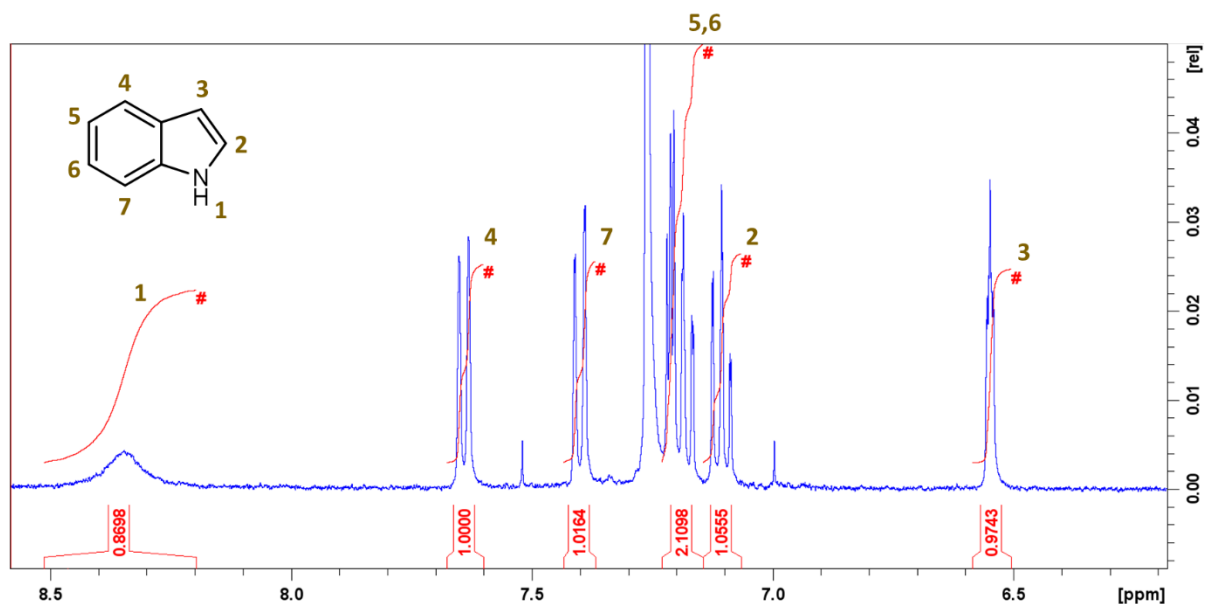


Figure S18. Dehydrogenation of indoline.

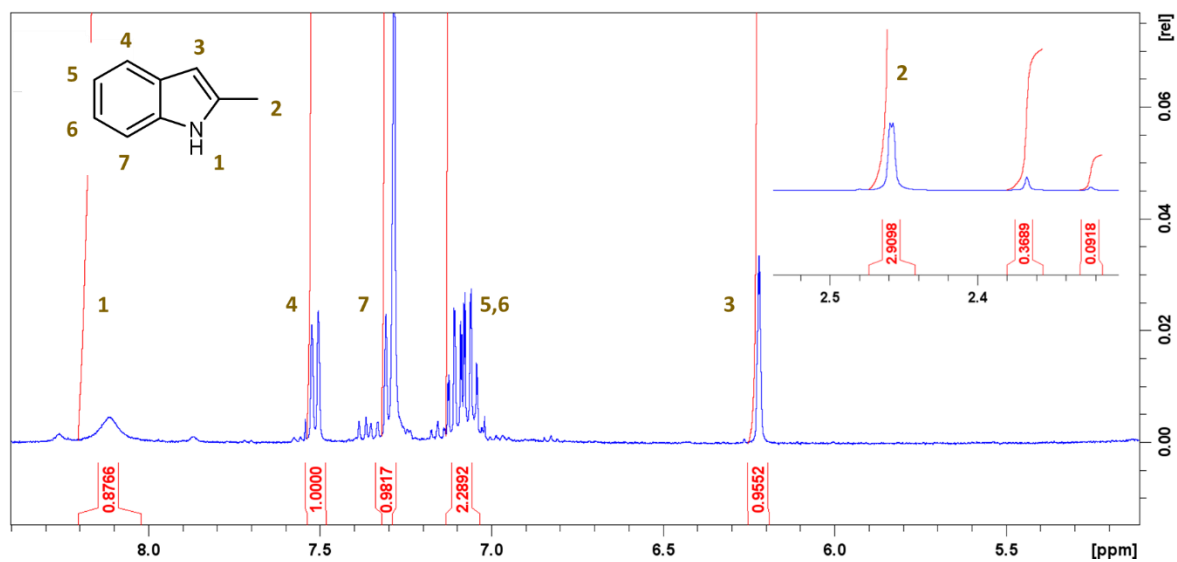


Figure S19. Dehydrogenation of 2-methylindoline.

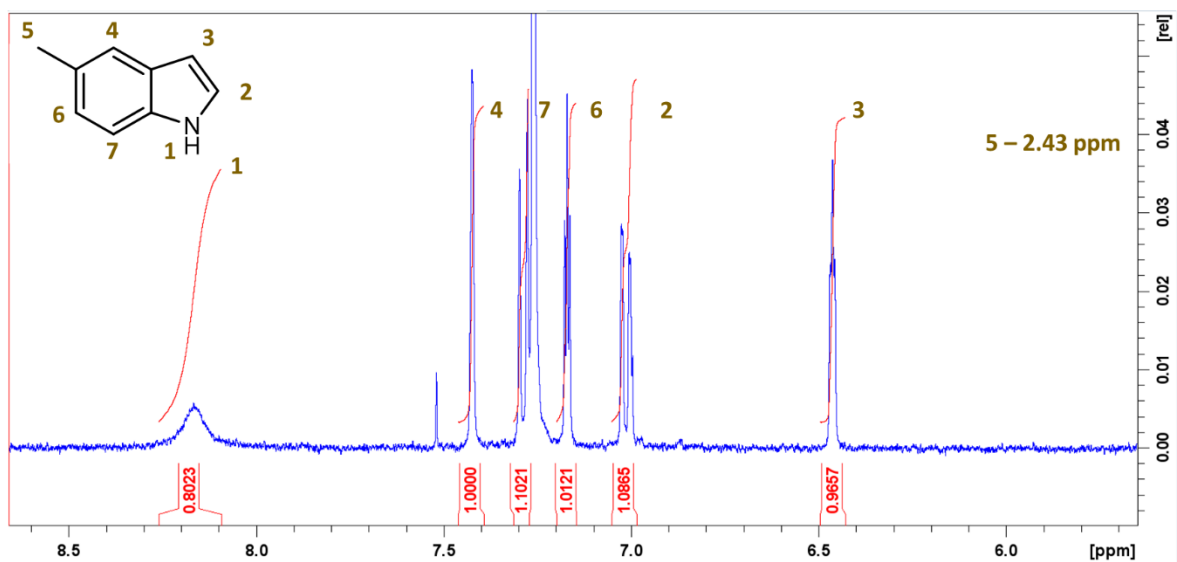


Figure S20. Dehydrogenation of 5-methylindoline.

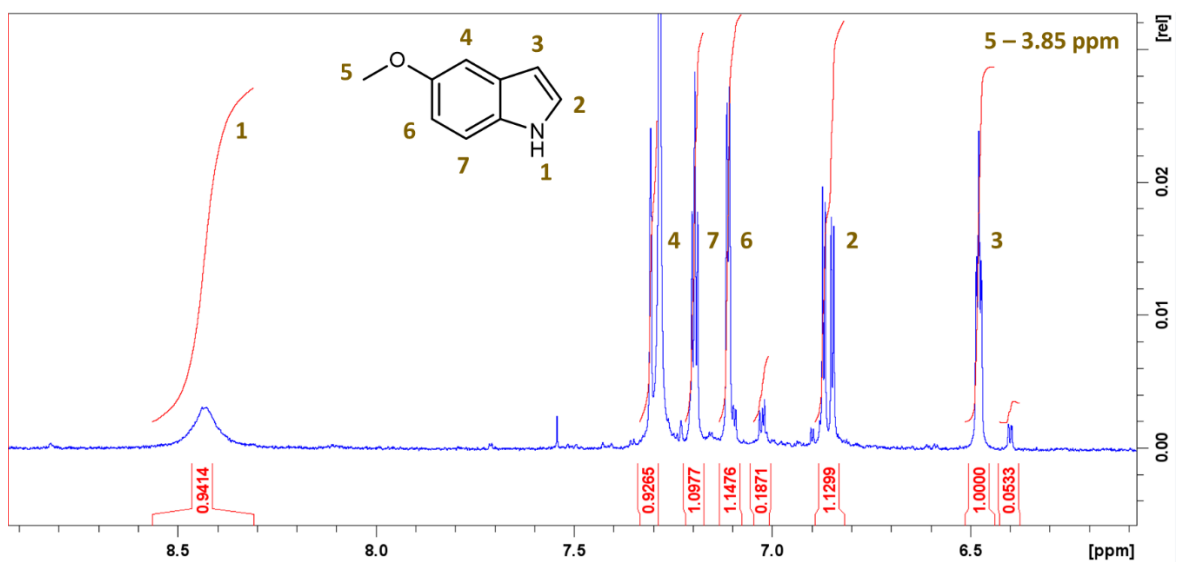


Figure S21. Dehydrogenation of 5-methoxyindoline.

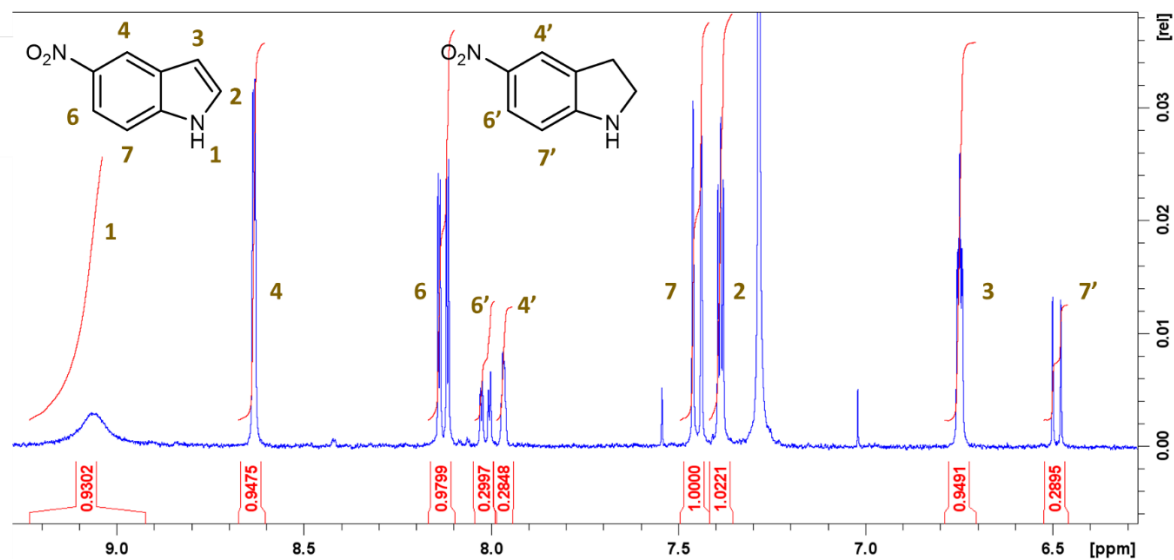


Figure S22. Dehydrogenation of 5-nitroindoline.

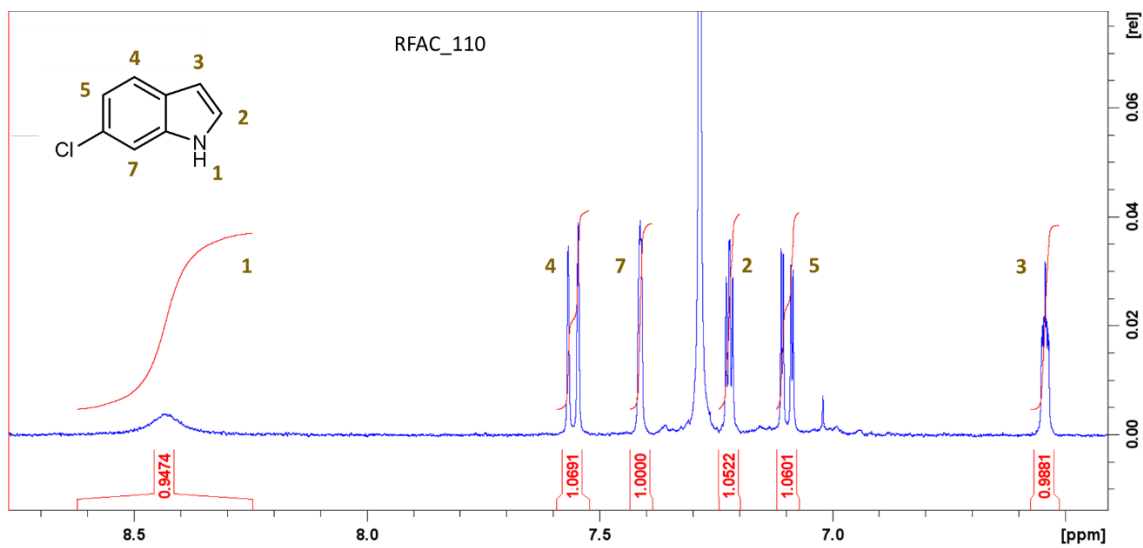


Figure S23. Dehydrogenation of 6-chloroindoline.

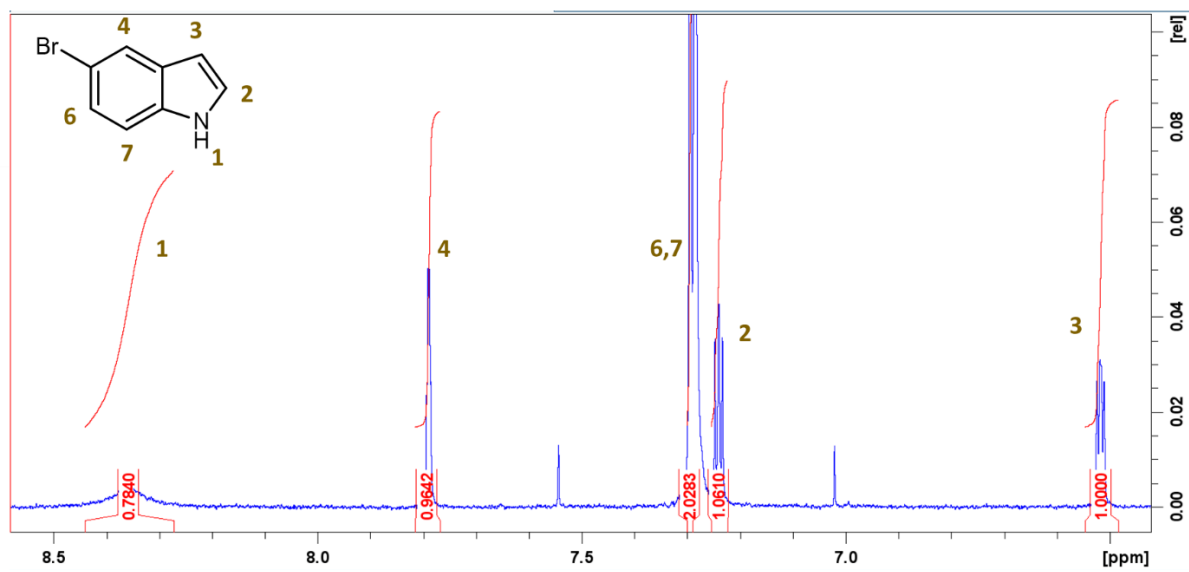


Figure S24. Dehydrogenation of 5-bromoindoline.

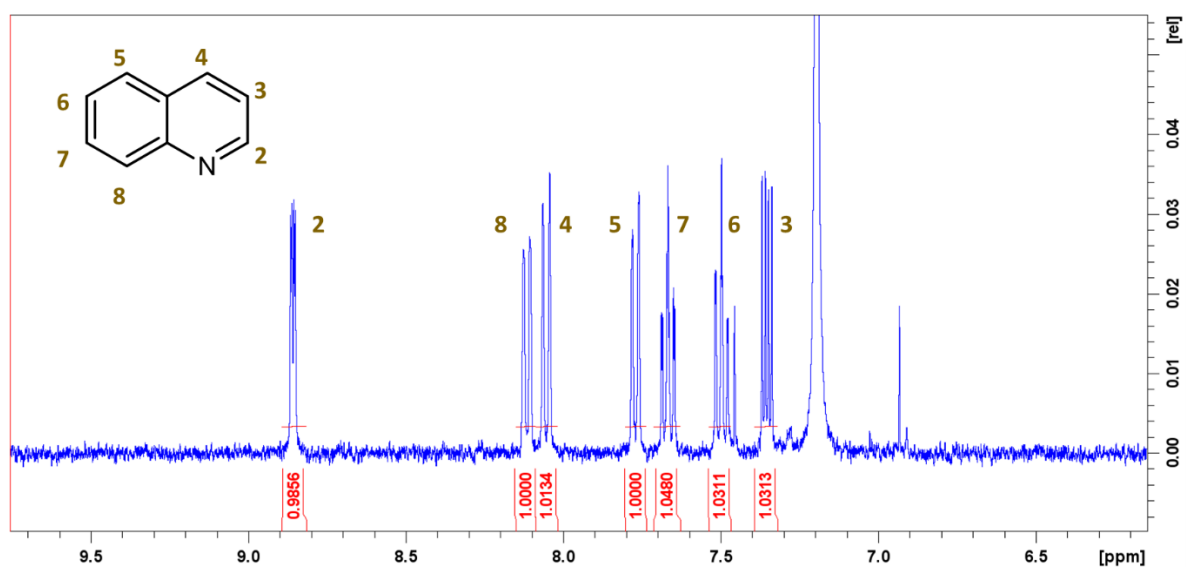


Figure S25. Dehydrogenation of tetrahydroquinoline.

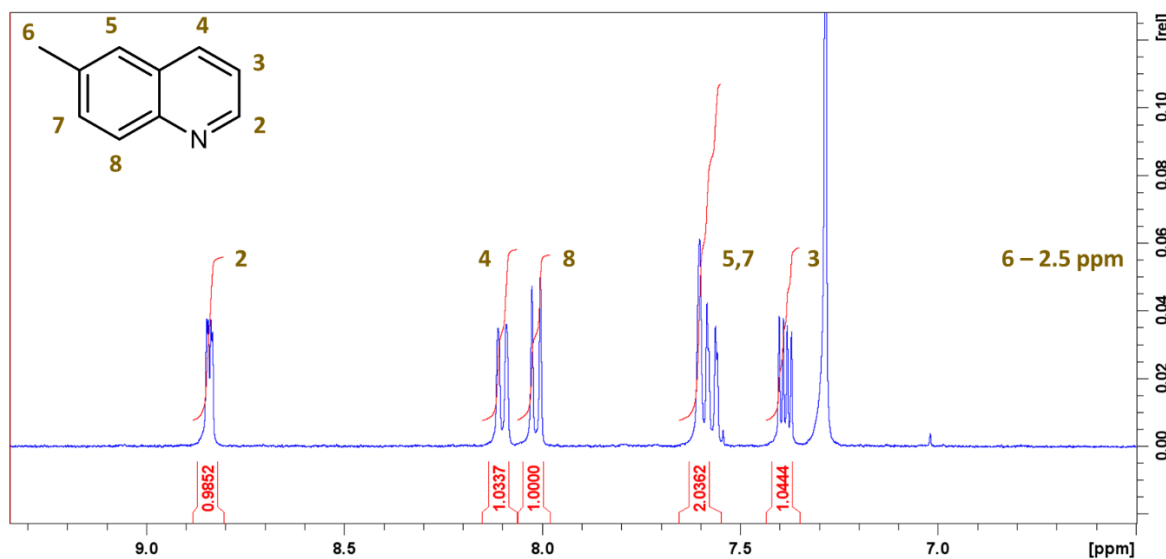


Figure S26. Dehydrogenation of 6-methyltetrahydroquinoline.

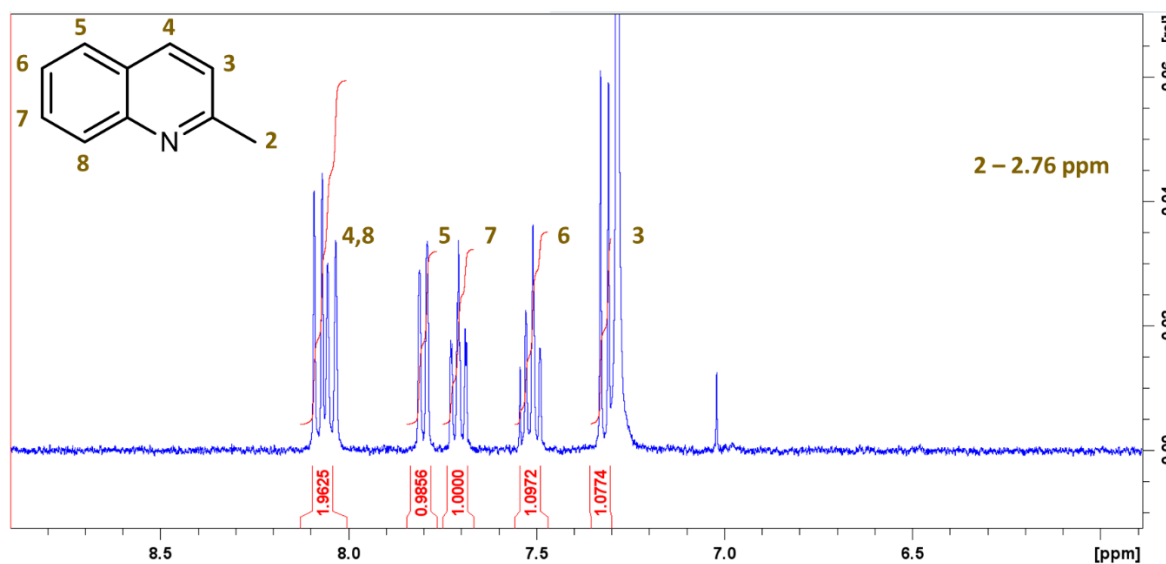


Figure S27. Dehydrogenation of 2-methyltetrahydroquinoline.

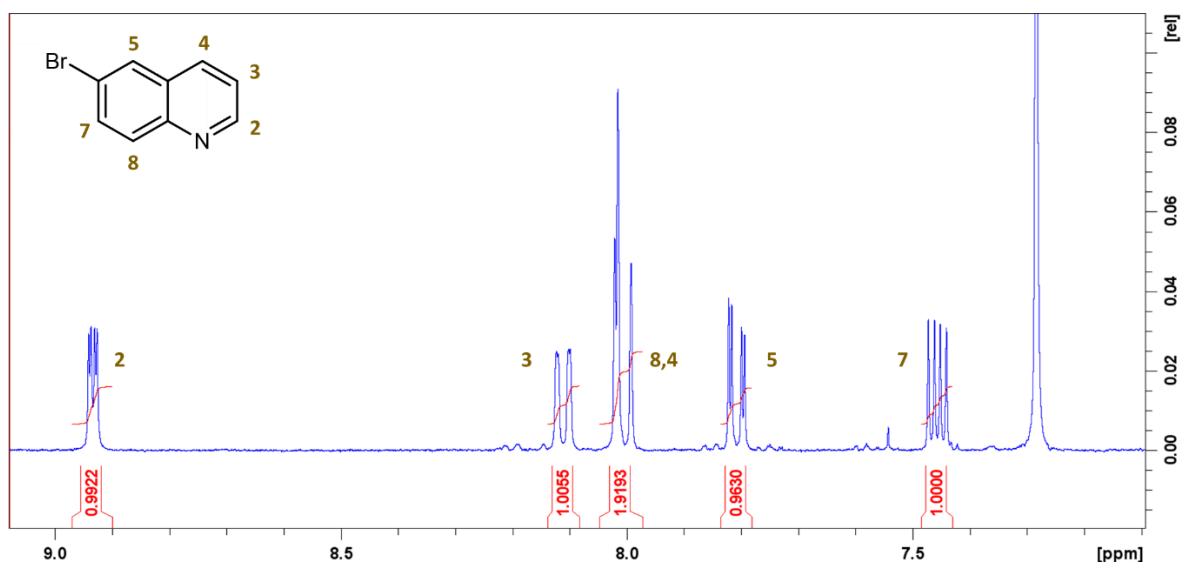


Figure S28. Dehydrogenation of 6-bromotetrahydroquinoline.

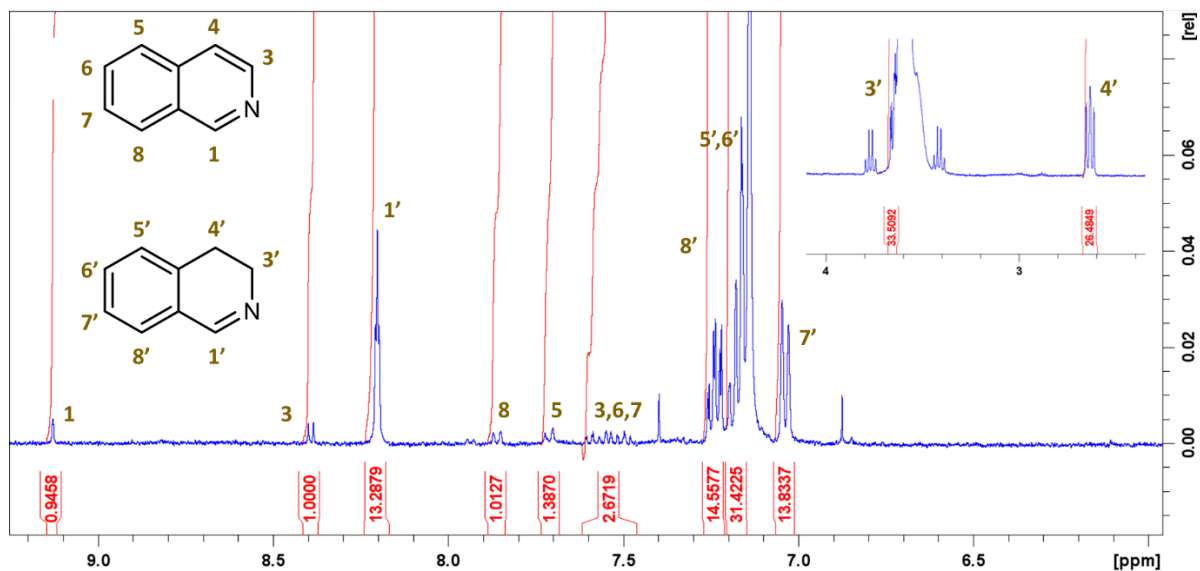


Figure S29. Dehydrogenation of tetrahydroisoquinoline.

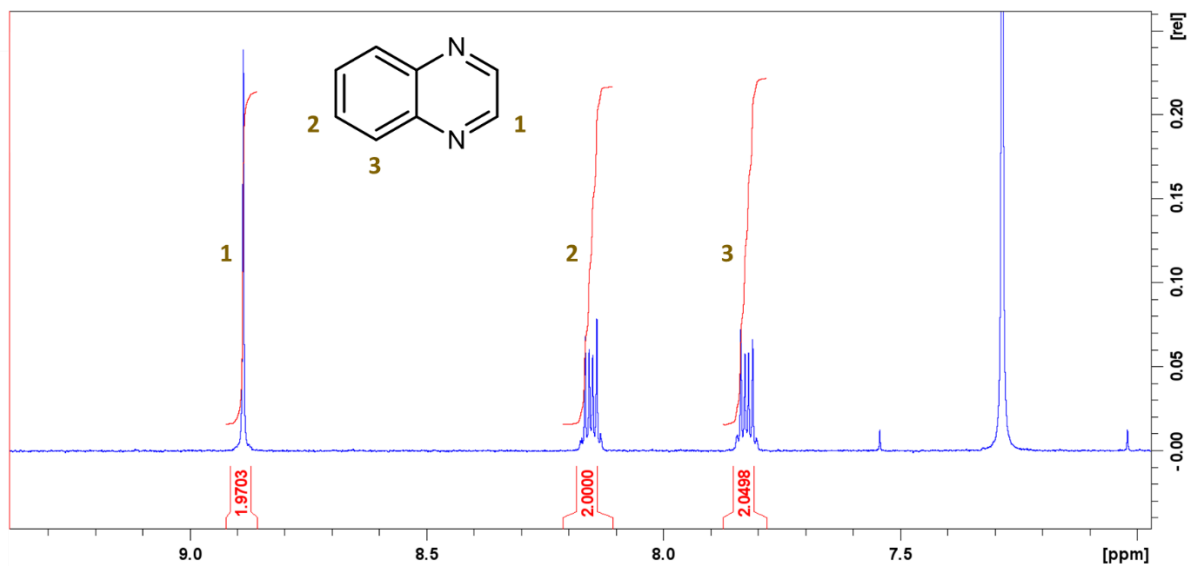


Figure S30. Dehydrogenation of tetrahydroquinoxaline.

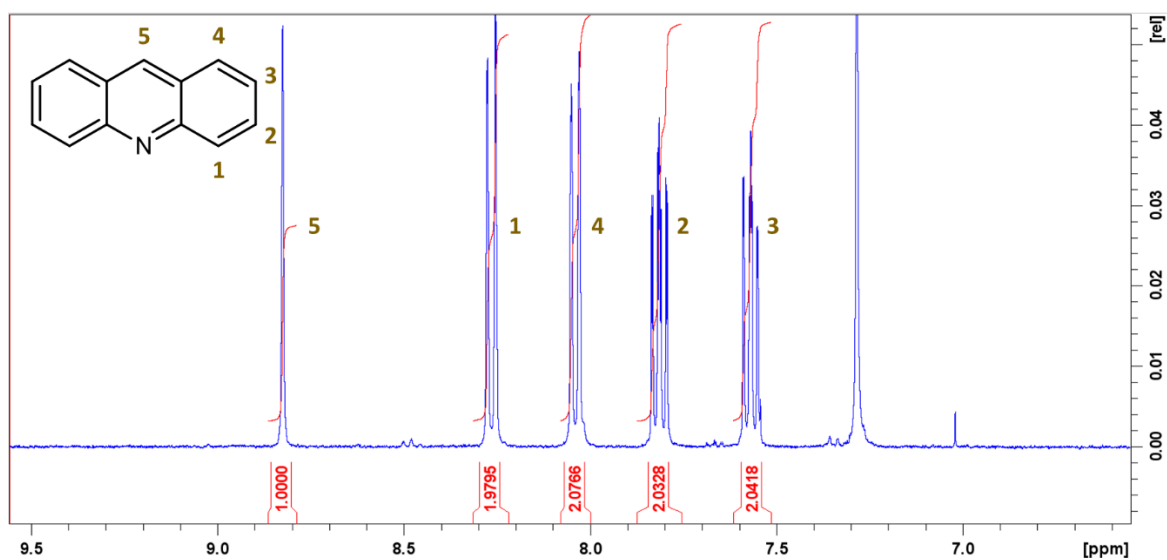


Figure S31. Dehydrogenation of 9,10-dihydroacridine.

C. Model materials

The P-doped carbon sample was synthesised by adapting Patel *et al.* work.⁶

Phytic acid, 50 wt.% in water (3.5 mL, 5 g, 3.78 mmol), was placed in a capped crucible disposed in a horizontal tubular oven. The mixture was subsequently submitted to a heat treatment at 700 °C (heating ramp: 2.5 °C/min) for 1 h under N₂ flux. After cooling down to r.t., the crude product was ground and washed two times with 400 mL deionized water for 8 h at r.t., before being dried in oven in air at 60 °C overnight. A black powder was obtained with a yield of 226 mg (71 % carbon yield).

The P content was estimated to be 5.4 wt.% by ICP.

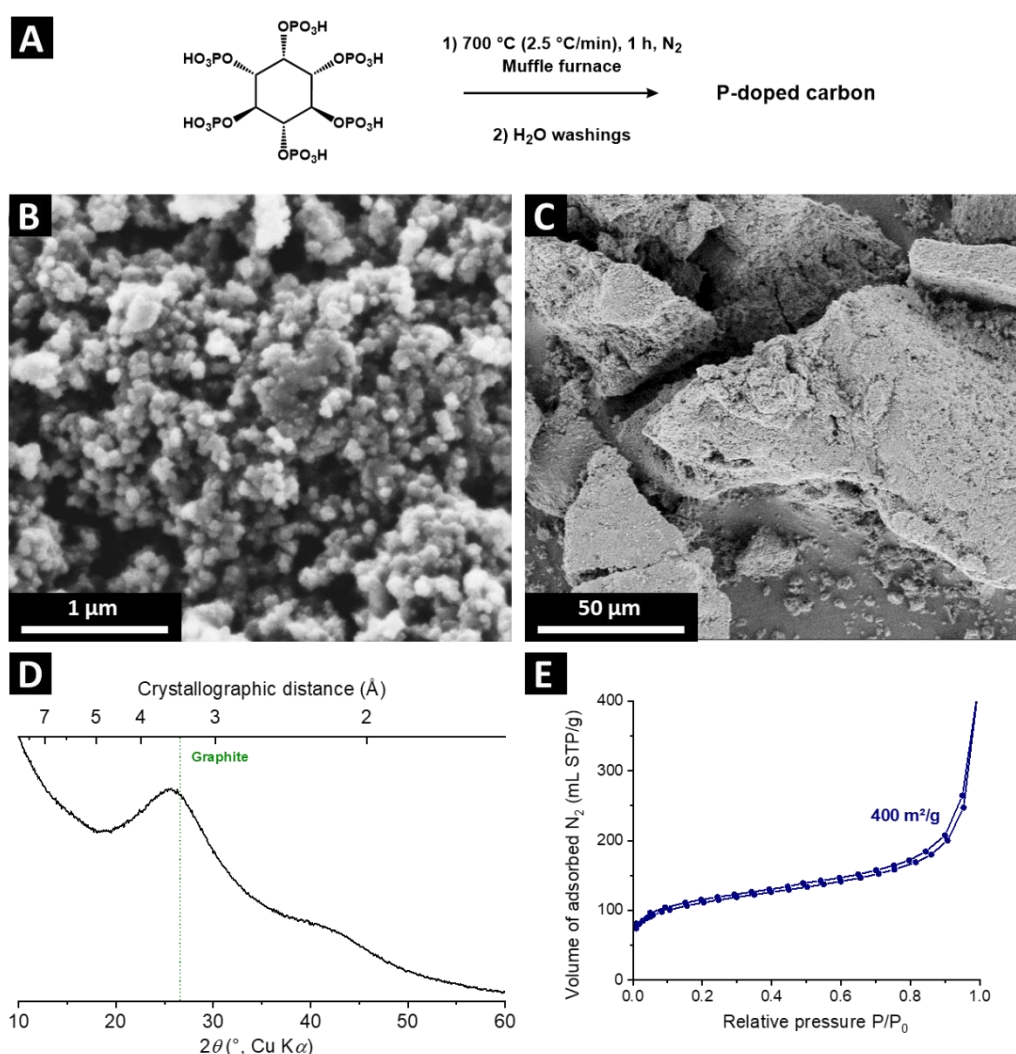


Figure S32. Synthesis of P-doped carbon. (A) Overall reaction. (B-C) SEM images. (D) X-ray diffractogram. (E) N₂ physisorption experiments performed at 77 K.

⁶ M. A. Patel, F. Luo, M. R. Khoshi, E. Rabie, Q. Zhang, C. R. Flach, R. Mendelsohn, E. Garfunkel, M. Szostak and H. He, *ACS Nano*, 2016, **10**, 2305-2315

The N-doped carbon sample was synthesised following Pampel *et al.* work.⁷

Adenine (5 g, 37.0 mmol) and MgCl₂·6H₂O (37.5 g, 184 mmol) were thoroughly mixed and placed in a capped ceramic crucible disposed in a muffle furnace. The mixture was subsequently submitted to a heat treatment at 700 °C (heating ramp: 2.5 °C/min) for 1 h under N₂ flux. After cooling down to r.t., the crude product was ground and washed two times with 400 mL HCl 1 M and one time with 400 mL deionized water for 8 h at r.t., before being dried in oven in air at 60 °C overnight. A black powder was obtained with a yield of 1376 mg.

The N content was estimated to be 24 wt.% by Elemental Combustion Analysis (ECA).

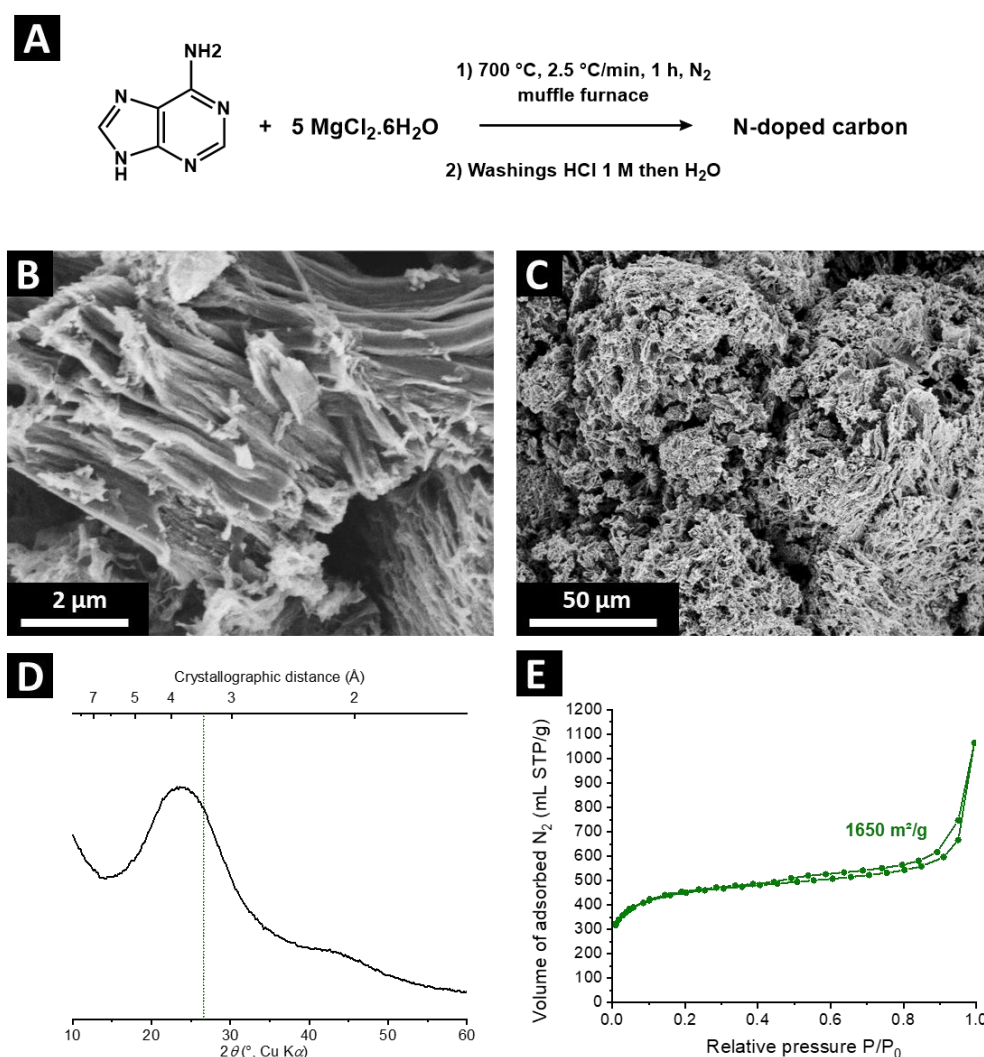


Figure S33. Synthesis of N-doped carbon. (A) Overall reaction. (B-C) SEM images. (D) X-ray diffractogram. (E) N₂ physisorption experiments performed at 77 K.

⁷ J. Pampel, A. Mehmood, M. Antonietti, T.-P. Feller, *Materials Horizons*, 2017,4, 493-501

The air-oxidized carbon black sample was synthesised following Enders *et al.* work.⁸

Carbon black (Ketjenblack® EC-600JD from Akzo Nobel) (500 mg) was placed in a capped ceramic crucible disposed in a muffle furnace. The mixture was subsequently submitted to a heat treatment at 450 °C (heating ramp: 5 °C/min) for 10 h in air. After cooling down to r.t., a black powder was obtained with a yield of 480 mg.

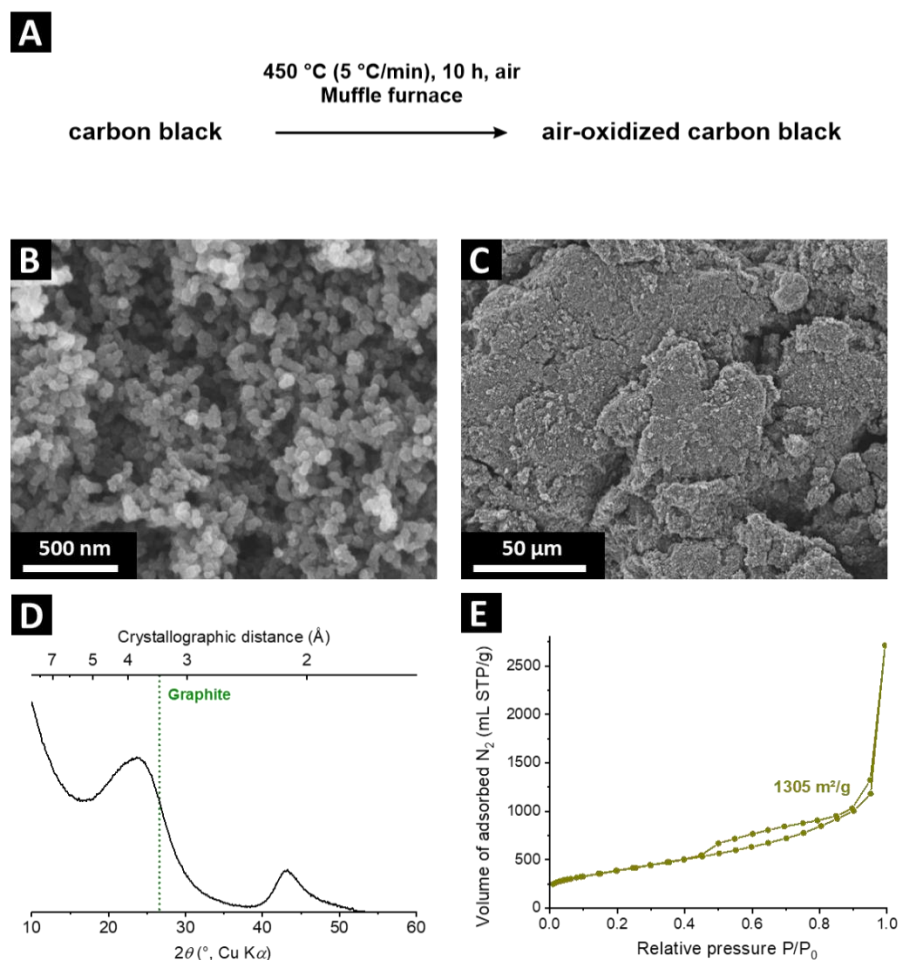


Figure S34. Synthesis of air-oxidized carbon black. (A) Overall reaction. (B-C) SEM images. (D) X-ray diffractogram. (E) N₂ physisorption experiments performed at 77 K.

⁸ L. Enders, ..., J. Helaja, *Catalysis Science & Technology*, 2021,**11**, 5962-5972

The phosphorylated carbon sample was synthesised by adapting J. Pampel work.⁹ The washing at the first step was performed in presence of ascorbic acid to generate –OH surface groups, prone for reaction with phosphoric acid.

Glucose (2.4 g, 13.3 mmol) and a prealably molten and ground KCl/ZnCl₂ eutectic (12 g) were thoroughly mixed and placed in a capped ceramic crucible disposed in a muffle furnace. The mixture was subsequently submitted to a heat treatment at 350 °C (heating ramp: 5 °C/min) for 2 h and 900 °C for 1 h under N₂ flux. After cooling down to r.t., the crude product was ground and washed one time with 400 mL deionized water and one time with 400 mL deionized water in presence of 2 g of ascorbic acid, for 8 h at r.t., before being dried in oven in air at 60 °C overnight. A black powder was obtained with a yield of 894 mg.

The resulting powder (727 mg) is subsequently dispersed by 30 min sonication in 6 mL of H₃PO₄ 85 % and heated in air at 180 °C for 6 h. After cooling down to r.t., the slurry was diluted to 50 mL with water, filtered and the powder washed three times with 400 mL deionized water for 8 h at r.t., before being dried in oven in air at 60 °C overnight. A black powder was obtained with a yield of 673 mg.

The P content was estimated to be 3.9 wt.% by ICP.

⁹ J. Pampel, C. Denton, T.-P. Fellingner, *Carbon*, 2016, **107**, 288-296

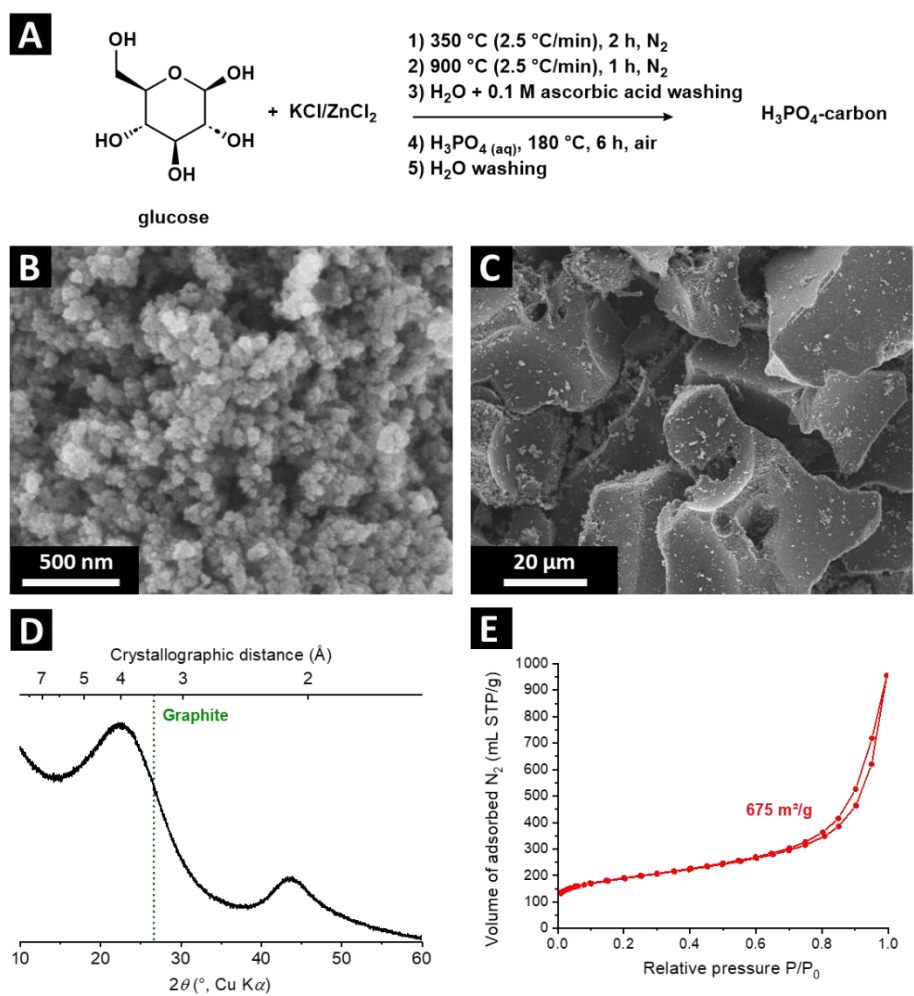


Figure S35. Synthesis of phosphorylated carbon. (A) Overall reaction. (B-C) SEM images. (D) X-ray diffractogram. (E) N₂ physisorption experiments performed at 77 K.